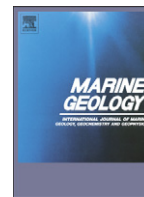




Contents lists available at ScienceDirect

## Marine Geology

journal homepage: [www.elsevier.com/locate/margeo](http://www.elsevier.com/locate/margeo)

## The Senegal River mud belt: A high-resolution archive of paleoclimatic change and coastal evolution

Jean Nizou<sup>a,\*</sup>, Till J.J. Hanebuth<sup>a</sup>, David Heslop<sup>a</sup>, Tilmann Schwenk<sup>a</sup>, Luisa Palamenghi<sup>a</sup>, Jan-Berend Stuut<sup>a,b</sup>, Rüdiger Henrich<sup>a</sup>

<sup>a</sup> MARUM, Department of Geosciences, University of Bremen, Klagenfurter Strasse, 28359 Bremen, Germany

<sup>b</sup> Royal Netherlands Institute for Sea Research, NL-1790 AB Den Burg, Texel, the Netherlands

### ARTICLE INFO

#### Article history:

Received 8 July 2009

Received in revised form 7 September 2010

Accepted 4 October 2010

Available online 12 October 2010

Communicated by J.T. Wells

#### Keywords:

mud depocenters

shelf sedimentation

Holocene climatic changes

NW-Africa

### ABSTRACT

Fine-grained sediment depocenters on continental shelves are of increased scientific interest since they record environmental changes sensitively. A north–south elongated mud depocenter extends along the Senegalese coast in mid-shelf position. Shallow-acoustic profiling was carried out to determine extent, geometry and internal structures of this sedimentary body. In addition, four sediment cores were retrieved with the main aim to identify how paleoclimatic signals and coastal changes have controlled the formation of this mud depocenter.

A general paleoclimatic pattern in terms of fluvial input appears to be recorded in this depositional archive. Intervals characterized by high terrigenous input, high sedimentation rates and fine grain sizes occur roughly contemporaneously in all cores and are interpreted as corresponding to intensified river discharge related to more humid conditions in the hinterland. From 2750 to 1900 and from 1000 to 700 cal a BP, wetter conditions are recorded off Senegal, an observation which is in accordance with other records from NW-Africa. Nevertheless, the three employed proxies (sedimentation rate, grain size and elemental distribution) do not always display consistent inter-core patterns. Major differences between the individual core records are attributed to sediment remobilization which was linked to local hydrographic variations as well as reorganizations of the coastal system.

The Senegal mud belt is a layered inhomogeneous sedimentary body deposited on an irregular erosive surface. Early Holocene deceleration in the rate of the sea-level rise could have enabled initial mud deposition on the shelf. These favorable conditions for mud deposition occur coevally with a humid period over NW-Africa, thus, high river discharge. Sedimentation started preferentially in the northern areas of the mud belt. During mid-Holocene, a marine incursion led to the formation of an embayment. Afterwards, sedimentation in the north was interrupted in association with a remarkable southward shift in the location of the active depocenter as it is reflected by the sedimentary architecture and confirmed by radiocarbon dates. These sub-recent shifts in depocenters location are caused by migrations of the Senegal River mouth. During late Holocene times, the weakening of river discharge allowed the longshore currents to build up a chain of beach barriers which have forced the river mouth to shift southwards.

© 2010 Elsevier B.V. All rights reserved.

### 1. Introduction

Fine-grained sediment bodies on continental shelves are considered as potential archives of past environmental changes, such as sea-level fluctuations, coastal morphodynamics or variations in terrigenous sediment input (e.g., Grossman et al., 2006; Hanebuth and Lantzsch, 2008). Whilst the terrigenous sediment supply to the

Senegalese continental shelf is controlled by both fluvial and aeolian primary inputs (Michel, 1973; Gac and Kane, 1986; Orange and Gac, 1990), numerous secondary factors have a potential effect on sediment deposition on the shelf, for example, sea level, oceanography, and exact position of the river mouth.

Shallow-acoustic profiling supplemented by elemental distribution, sedimentation rate calculations, and grain-size distribution data obtained from four sediment cores retrieved from the mud belt adjacent to the Senegal River are used here to quantify the extent to which coastal and paleoclimatic changes have been recorded in this shelf deposit during the Holocene. In addition to a reconstruction of the paleoclimatic influence, a link between the build-up of this shelf

\* Corresponding author.

E-mail address: [nizou@uni-bremen.de](mailto:nizou@uni-bremen.de) (J. Nizou).

deposit, the local coastal dynamics and the evolution of the Senegal River flood plain is established and a paleogeographic reconstruction is proposed.

## 2. Regional settings

### 2.1. Primary sediment supply to the Senegalese shelf

Offshore Senegal, primary sediment input is derived from two sources: fluvial material from the Senegal River and dust particles from the arid Saharan and semi-arid Sahelian belts (Michel, 1973; Gac and Kane, 1986; Orange and Gac, 1990). The Senegal River alluvial valley covers an area of  $\sim 0.343 \times 10^6 \text{ km}^2$  (Fig. 1C). The average water discharge over the year at the last downstream point prior to the estuary (Dagana) is  $\sim 641 \text{ m}^3/\text{s}$ , however, this discharge is highly seasonal due to the monsoonal conditions. Interannual rainfall variability over NW-Africa is controlled by the monsoon. During boreal

summer (June to August), the Intertropical Convergence Zone and its associated Tropical Rain Belt migrate northwards (up to  $19^\circ\text{N}$ ) and bring moisture-laden air over the Senegal River basin. During winter (December to February), the Intertropical Convergence Zone migrates toward the South (down to  $5^\circ\text{N}$ ) which induces cool and dry conditions over the Senegal River basin (Leroux, 2001). The annual sediment load delivered to the coast is around  $2 \times 10^6 \text{ t}$  (Gac and Kane, 1986). The generally low flow regime combined with a river bed which is situated in some areas below sea level, allowed ocean waters to intrude up to Bogué before the construction of the Diama dam in 1985 (Fig. 1C).

The aeolian component of sediment supply is also significant. Two wind systems deliver dust material to the final place of deposition off Senegal (e.g., Sarnthein et al., 1981; Stuut et al., 2005). During the cool and dry boreal winter ( $22^\circ\text{C}$  and  $0 \text{ mm}$  precipitation in January in average), the NE Trade winds are the dominant atmospheric feature. In contrast, during summer ( $27^\circ\text{C}$  and  $254 \text{ mm}$  precipitation in

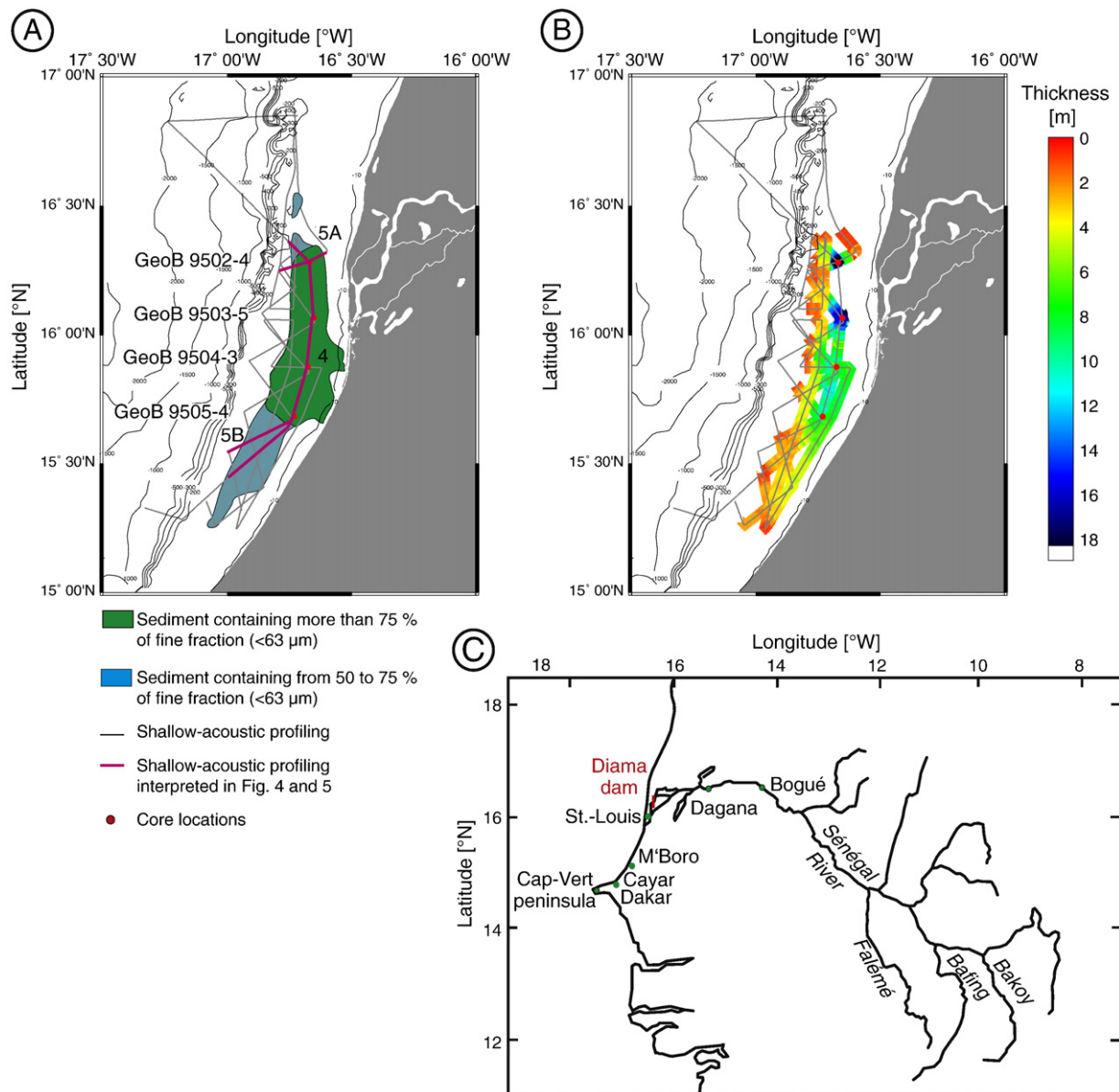


**Fig. 1.** (A) Bathymetric map of the studied area displaying the seismic profiling, the core locations and two types of mud cover based on their proportion of fine fraction (redrawn after Domain, 1977). Capital letters correspond to the profiles interpreted in Figs. 4 and 5. (B) Isopach map displaying the thickness of the MB along the shallow-acoustic profiles. Core sites are also displayed, from North to South: GeoB9502-4, 9503-5, 9504-3, 9505-4. (C) Map showing the water course of the Senegal River and its main tributaries.

August in average), strong Earth-surface turbulence associated with the monsoonal front system lifts the dust from a height of 3000 to 7000 m and the material is transported westward by the Sahara Air Layer (see [Stuut et al., 2005](#) for a review). Prominent dust source regions frequently suggested in the literature are the Bodélé depression (Chad; [Washington et al., 2006](#)) and a low relief area extending over eastern Mauritania, western Mali and southern Algeria ([McTainsh and Walker, 1982](#)).

## 2.2. Oceanography of the Senegalese shelf

The current regime on the Senegalese shelf behaves also highly seasonal. In winter time ([Fig. 2B](#)), cool (18–19 °C) and saline (35.5‰ psu) surface waters deriving from a component of the southward flowing coastal Canary Current and from a series of upwelling cells off Morocco and Mauritania are forced to the S–SW by the NE Trade winds ([Domain and Bouille, 1976; Rebert, 1979](#); ~50 cm/s flow speed in average). This current extends over the entire shelf with an intensive water column mixing down to 50 m. During summer time ([Fig. 2A](#)), a component of the warm Equatorial Counter Current (27–28 °C; 37.5‰ psu) flows northward onto the shelf. This surface current is weaker than the wintery flow regime and prone to large wind-induced fluctuations in speed ([Domain and Bouille, 1976; Rebert, 1979](#); ~25 cm/s flow speed in average). The effect of both seasonal current regimes on shelf sedimentation is, however, poorly understood yet.

The tides in this region are semi-diurnal with mean amplitude ranging from 0.55 to 1.15 m ([Faure et al., 1980](#)). The tidal-induced currents are weak and, thus, do not notably affect the sediment transport on the continental mid-shelf ([Domain and Bouille, 1976](#); ~10 to 15 cm/s flow speed in average).

Off the Senegalese coast, two types of swell systems occur. A dominant high-energy NW swell with a direction of propagation that fluctuates from 10° to 30° N disturbing the water column down to 30 m (wave length of 300 m, oscillation period varying from 8 to 12 s, height of 1 m, and speed of 21 m/s; [Pinson-Mouillot, 1980](#)). A second, weaker SW swell displays less variability in propagation direction

(oscillation period ranges from 5 to 8 s, height of 0.8 m). This subordinate swell may interfere with the dominant one enhancing or diminishing the littoral drift ([Masse, 1968; Pinson-Mouillot, 1980](#)). This strong littoral drift is oriented toward the south ([Barusseau et al., 1998](#); ~30 cm/s flow speed in average). The resulting direct littoral sand transit occurs down to 2.5 m water depth ([Monteillet, 1988](#)). The combination of the latter with the wave regime leads to the development of extended systems of sand spits, beach barriers and wide sand beaches along the coasts.

## 2.3. Present-day configuration of the offshore and onshore Senegal River mouth system

North of Cap-Vert peninsula, the continental shelf off Senegal displays different morphologies. From Cayar to M'Boro, the shelf is narrow (~20 km), shows a slope ranging from 1.8 to 0.3% and hosts two canyons the Cayar canyon (off Cayar) and the Djoloff canyon (off M'Boro), which cut back into the outer shelf. From M'Boro to the Senegal River mouth the shelf widens significantly (~40 km), its slope decreases down to 0.2% and hosts the Peul canyon (off Lompoul). North of the Senegal River mouth, the shelf narrows again ([Pinson-Mouillot, 1980](#)). The shelf break is situated on average at a water depth of 100 m. Major parts of this shelf are dominated by bioclastic sands, however, [Domain \(1977\)](#) and [Seibold and Fütterer \(1982\)](#) have observed a defined muddy area in mid-shelf position which is characterized by more than 75% of fine-grained sediments ([Fig. 1A, B](#)). We, therefore, refer to this fine-grained sedimentary depocenter as a mud belt (MB) in the following.

The sandy Senegalese coast is oriented N–S from Mauritania to the southernmost extension of the Langu de Barbarie, and from this point towards the south, the coast is NE–SW oriented ([Fig. 1](#)). The terminal reach of the Senegal River is separated from the open Atlantic Ocean by sand bodies, with the Langu de Barbarie being the southernmost and youngest of these sand spits ([Monteillet, 1988](#)). From the coastline towards the hinterland a succession of three dune systems can be observed ([Pinson-Mouillot, 1980](#)). (1) Present-day dunes are arranged in a 100 to 1200 m-wide strip parallel to the coast.

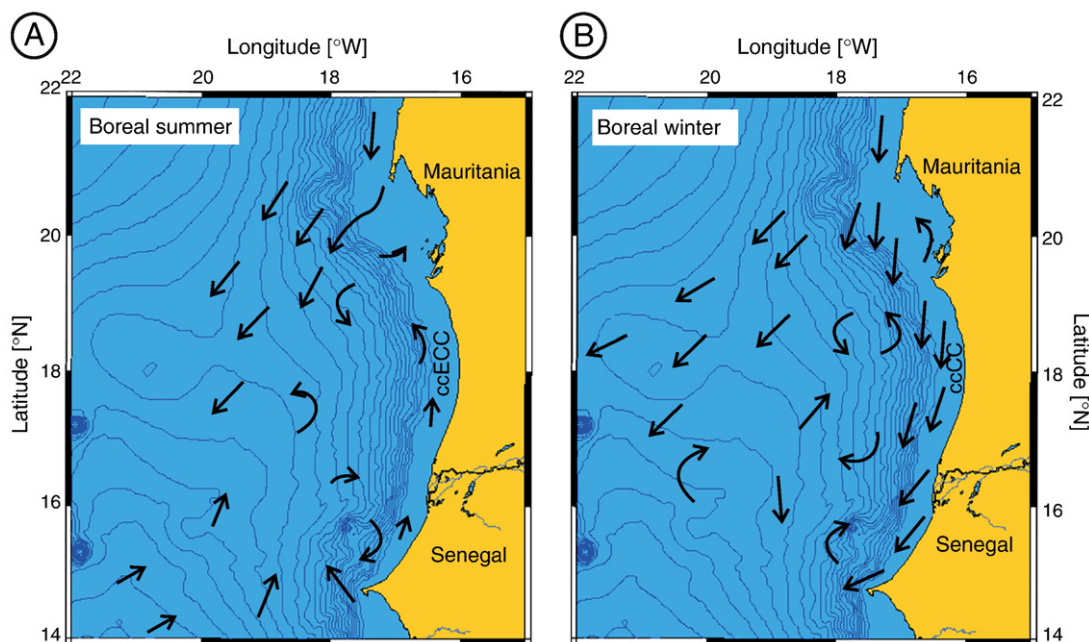


**Fig. 2.** The current regime on the Senegalese shelf for each season redrawn after [Rebert \(1979\)](#). Coastal component of the Equatorial Counter Current (ccECC) and the coastal component of the Canary Current (ccCC) are displayed.

(2) Yellow dunes display several shapes that are parabolic, barchans (crescentic), star and linear shaped. (3) Red “Ogolien” dunes can be classified in two types: reworked and fixed (Pinson-Mouillot, 1980). Reworked red dunes are oriented from NNW–SSE to WNW–ESE and show depressions called Niayes. Niayes are of dual origin: inter-dune depressions (*sensu stricto*) and fossil of fluvial channel networks. Further inland, fixed red dunes are NE–SW oriented and their associated inter-dunes are covered by vegetation (Pinson-Mouillot, 1980). Inland, a wide alluvial plain is characterized by morpho-sedimentary structures typical for fluvial environments such as channel networks bounded by levees, and depressions where clays settle down (Michel, 1973).

2.4. History of regional sea-level fluctuations

For the Senegalese coast, Faure et al. (1980) have proposed a sea-level reconstruction which was estimated by <sup>14</sup>C-dated fossil assemblages (Fig. 3; Table 1). This reconstruction is assumed to document a sea-level highstand around 5500 cal a BP and a subsequent regression with two minor peaks above modern sea level at around 2850 and 1700 cal a BP. Such an observation is in accordance with many worldwide-distributed low-latitude sea level reconstructions (e.g., Clark et al., 1978; Pirazzoli and Montaggioni, 1988; Haworth et al., 2002; Lambeck, 2002). In contrast some studies suggest that the so-called “nouakchttian transgression” (e.g., Barousseau et al., 1995) with an elevation estimated around 2 to 3 m for the coasts of the Senegalo-Mauritanian lowlands during the mid-Holocene was a marine incursion linked to climatic and morpho-sedimentary phenomena (Ausseil-Badie et al., 1991; Barousseau et al., 2007; Vernet, 2007; Barousseau et al., 2009).

Monteillet et al. (1981) have suggested that a marine incursion into the lower Senegal River valley could also have appeared due to a climate-related reduction of fresh-water input. This is supported by the shoreline geometry and the flat coastal topography of the region which could have favored salt-water intrusions and allowed deposition of shells during dry periods especially during high tides (tides range: 0.55–1.15 m). The peaks (50 cm above modern sea level) assumed by Faure et al. (1980) at around 2850 and 1700 cal a BP could have occurred during drought conditions, thus reduced fresh-water

Table 1

Recalibration of the dates used for the sea-level reconstruction by Faure et al. (1980). All radiocarbon dates were calibrated by the program CALIB 5.0.1. (Stuiver et al., 1998).

Lab no.	Material	Paleo sea-level [m]	<sup>14</sup> C age [a BP]	1 σ-calibrated [cal a BP]	Intercept [cal a BP]
(Rk 3D)	Shells	-0.5 ± 0.7	6970 ± 90	7705–7922	7815
I-2928	<i>A. senilis</i>	-0.5 ± 1	6740 ± 130	7476–7695	7585
Gif-4260	<i>A. senilis</i>	-1 ± 1	6540 ± 130	7325–7566	7445
(Rk 5)	<i>A. senilis</i>	0 ± 1	6520 ± 100	7324–7553	7440
Gif-4261	<i>A. senilis</i>	-0.5 ± 1	6360 ± 130	7166–7424	7295
Ly-1930	Peat	0 ± 0.5	6060 ± 150	6748–7156	6950
(R 3)	Peat	-0.5 ± 0.7	5895 ± 250	6413–7003	6710
(Rk 3B)	<i>A. senilis</i>	0.1 ± 0.7	5700 ± 90	6405–6629	6515
Ly-1345	<i>A. senilis</i>	-0.7 ± 1	5670 ± 240	6210–6776	6495
Ly-985	<i>A. senilis</i>	0 ± 0.5	5650 ± 150	6300–6629	6465
Ly-987	<i>A. senilis</i>	0 ± 0.5	5590 ± 140	6217–6552	6385
T-463	<i>A. senilis</i>	0.5 ± 0.5	5470 ± 110	6123–6403	6265
(Rk 6)	<i>A. senilis</i>	0 ± 1	5465 ± 120	6029–6402	6215
Ly-983	<i>A. senilis</i>	0 ± 0.5	5250 ± 120	5913–6184	6050
MC-1562	<i>A. senilis</i>	0 ± 0.5	5070 ± 120	5662–5921	5790
Gif-1450	Peat	0.4 ± 0.5	4750 ± 130	5319–5599	5460
Ly-986	<i>A. senilis</i>	1 ± 0.5	4720 ± 140	5296–5606	5450
Ly-982	<i>A. senilis</i>	1 ± 0.5	4670 ± 120	5150–5585	5370
Ly-1344	<i>A. senilis</i>	0.5 ± 0.5	4220 ± 160	4523–4968	4745
I-2774	<i>A. senilis</i>	1 ± 1	4080 ± 120	4436–4813	4625
MC-1563	Shells	0.3 ± 1	4010 ± 110	4296–4797	4545
I-2294	<i>A. senilis</i>	0 ± 1	3970 ± 105	4245–4569	4405
Gif-4259	<i>A. senilis</i>	0 ± 1	3430 ± 100	3577–3829	3705
Ly-984	<i>T. fuscatus</i>	-0.3 ± 0.5	3410 ± 130	3485–3831	3660
I-2298	<i>A. senilis</i>	0 ± 1	3250 ± 110	3366–3613	3490
I-2297	Shells	0.5 ± 1	2710 ± 100	2744–2944	2845
I-2295	<i>A. senilis</i>	0 ± 1	2470 ± 110	2367–2710	2540
(F 3)	<i>T. fuscatus</i>	0.5 ± 1	1980 ± 100	1820–2095	1960
I-2296	Shells	0.5 ± 1	1880 ± 100	1702–1941	1820
(F9A)	<i>T. fuscatus</i>	0.5 ± 1	1860 ± 120	1625–1929	1775
Gif 363	<i>A. senilis</i>	0.6 ± 1	1620 ± 120	1386–1690	1540
(F 8)	<i>T. fuscatus</i>	0.5 ± 1	1545 ± 120	1316–1543	1430

discharge by the Senegal River (Bouimetarhan et al., 2009). Salt-water intrusions favored by high tides and low river discharge may have deposited shells inland, leading to these two peaks.

3. Materials and methods

3.1. Material

The four sediment gravity cores GeoB 9502-4 (16°16.90'N; 16°40.20'W; 63 m water depth; 557 cm recovery), 9503-5 (16°03.99'N; 16°39.15'W; 50 mwd; 792 cm), 9504-3 (15°52.59'N; 16°40.50'W; 43 mwd; 560 cm) and 9505-4 (15°41.00'N; 16°43.88'W; 36 mwd; 530 cm) during the Senegal MB during the RV METEOR cruise M65-1 in June 2005 (Fig. 1A,B; Table 2). In addition, four 50-cm long multi-cores were taken at the same stations to obtain undisturbed seabed surface material. Lithology and sediment texture of the four gravity cores are rather comparable. They are composed of dark olive green sediment, only slightly bioturbated and containing small numbers of carbonate shell fragments throughout the cores (Mulitza et al., 2005).

Table 2

Core locations, core lengths and water depth at which they were retrieved.

GeoB	Latitude [°N]	Longitude [°W]	Length [cm]	Water depth [m]
9502-4	16°16.90	16°40.20	557	63
9503-5	16°03.99	16°39.15	792	50
9504-3	16°03.99	16°39.15	47	49
9504-3	15°52.59	16°40.50	560	43
9504-4	15°52.59	16°40.50	50	43
9505-4	15°41.00	16°43.88	530	36

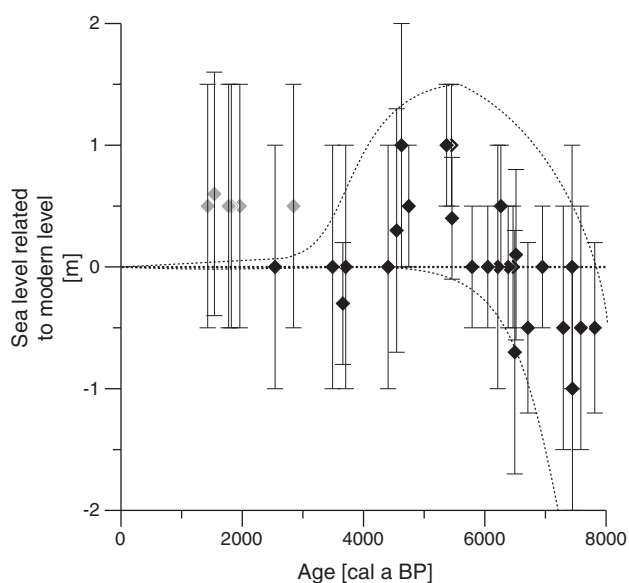


Fig. 3. Ages stem from the Faure et al. (1980) sea-level reconstruction. Dates were calibrated by the program CALIB 5.0.1. (Stuiver et al., 1998) using an atmospheric calibration (Table 1). Dashed lines enveloping the data represent two possible end-members of sea-level reconstruction.

**Table 3**

Radiocarbon measurements and age calibrations. All AMS-radiocarbon dates were calibrated by the program CALIB 5.0.1. (Stuiver et al., 1998).

Lab no.	Core no. (GeoB)	Depth in core [cm]	<sup>14</sup> C age [conv. a BP]	1 $\sigma$ -calibrated [cal a BP]	Intercept [cal a BP]
KIA 33735	9502-4	4	895 ± 25	513–532	525
KIA 33737	9502-4	230	2305 ± 35	1820–1890	1855
KIA 33738	9502-4	410	2850 ± 30	2365–2691	2525
KIA 33736	9502-4	575	2535 ± 30	2060–2286	2175
KIA 33732	9503-3	1	0	0	0
KIA 33739	9503-3	44	2315 ± 30	1825–1887	1855
KIA 28454	9503-5	20	1675 ± 30	1179–1266	1225
KIA 29768	9503-5	70	1870 ± 30	1320–1383	1350
KIA 29767	9503-5	140	2310 ± 30	1824–1883	1855
KIA 28452	9503-5	213	2555 ± 30	2070–2299	2185
KIA 29766	9503-5	320	2655 ± 30	2183–2336	2260
KIA 29765	9503-5	410	2740 ± 30	2335–2358	2345
KIA 28451	9503-5	529	2925 ± 30	2515–2733	2625
KIA 29764	9503-5	600	2965 ± 30	2620–2748	2685
KIA 29763	9503-5	700	3600 ± 30	3391–3445	3420
KIA 28450	9503-5	780	4140 ± 35	3999–4150	4075
KIA 33733	9504-4	1	0	0	0
KIA 33734	9504-4	48	945 ± 30	527–622	575
KIA 30522	9504-3	5	1175 ± 40	678–725	700
KIA 33727	9504-3	173	1605 ± 45	1063–1178	1120
KIA 33728	9504-3	238	2240 ± 45	1716–1823	1770
KIA 33729	9504-3	298	2400 ± 45	1897–1993	1945
KIA 33730	9504-3	373	2640 ± 30	2163–2330	2245
KIA 33731	9504-3	498	3060 ± 30	2749–2780	2765
KIA 30512	9504-3	557	3275 ± 40	2948–3072	3010
KIA 33740	9505-4	4	0	0	0
KIA 33741	9505-4	132	810 ± 60	330–518	425
KIA 33742	9505-4	378	1750 ± 30	1271–1300	1285
Poz-22942	9505-4	510	3645 ± 30	3405–3551	3480

Shallow-acoustic profiles were retrieved during METEOR cruise M65/1 in June 2005 and during MERIAN cruise MSM11/2 in March/April 2009. The shipboard Parasound system is a parametric sediment echosounder (Grant and Schreiber, 1990). This system emits two primary signals with frequencies of 18 kHz and 22 kHz producing thereby a secondary (parametric) signal of 4 kHz. Parasound profiles

were collected in a zigzag cruise track along and across the Senegal MB (Fig. 1A). The data were processed in Kingdom Suite 8.0 in order to establish distribution maps and isopach maps.

### 3.2. Methods

In order to avoid dating problems with regard to redeposition processes, only well-preserved carbonate shells were carefully selected for dating. The age models are derived from 29 AMS-<sup>14</sup>C dates measured at the Leibniz Laboratory in Kiel (Germany), and the Poznań Radiocarbon Laboratory (Poland). The raw dates were calibrated using CALIB 5.0.1. (Stuiver et al., 1998). A 400-year marine reservoir age was subtracted from the conventional <sup>14</sup>C age and the atmospheric calibration curve was applied (Table 3). All ages are given in calibrated years before present (cal a BP) in the following. The age models and the associated sedimentation rates of the four cores are based on a linear interpolation between calibrated radiocarbon ages (data shown are available on <http://www.pangaea.de>).

To allow a reliable comparability, the <sup>14</sup>C dates used for the sea-level reconstruction by Faure et al. (1980) were calibrated (Fig. 3; Table 1). The material used by Faure et al. (1980) were bivalves (*Arca senilis*) which are common in shallow lagoons and estuaries, as well as gastropods (*Tympanotunus fuscatus*) and mangrove peats from the inter-tidal zone. The vicinity to the Senegal River would, however, suggest a possibly strongly reduced reservoir age. Therefore, we used an atmospheric calibration without reservoir correction being aware that the reservoir age correction is a critical issue for shelf waters as well as for coastal zones.

The X-ray fluorescence core scanner (Avaatech, The Netherlands) provides semi-quantitative bulk-sediment element-distribution data by non-destructive measurement at 1-cm resolution. We use a ratio of two selected elements to avoid dilution effects, with Fe/Ca being particularly valuable for stratigraphic purposes as Fe is considered to be of terrigenous origin and Ca, stemming from calcareous tests, of marine origin. Fe is a redox-sensitive element, however in front of the Senegal River, the very high sedimentation rates make the diagenetic alteration processes of minor importance compared to the

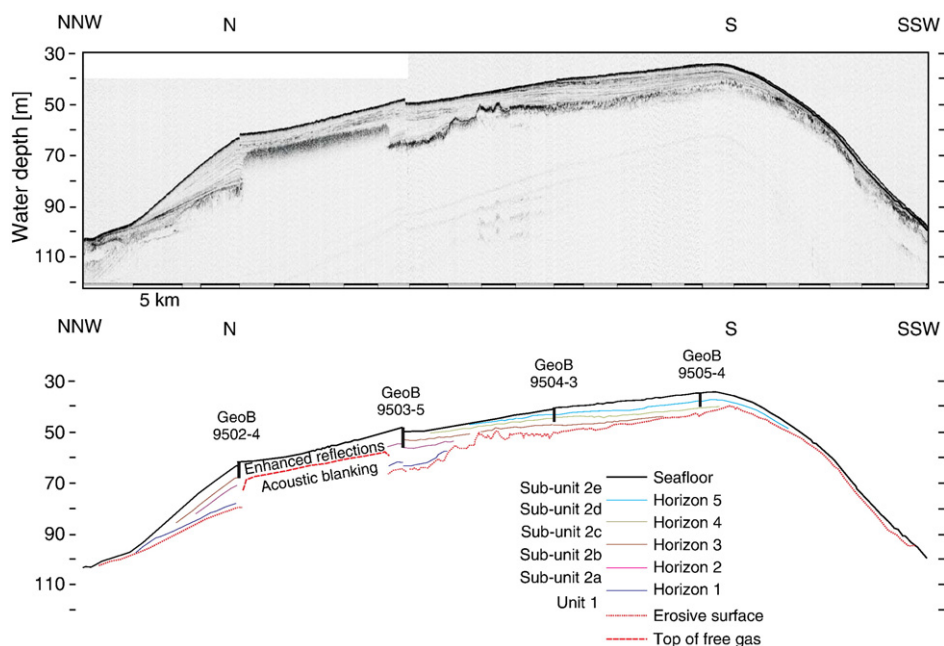


**Fig. 4.** Parasound profile of north-south transects (Fig. 1A) along the coast. An interpretation of the deposit architecture is displayed below each profile as well as length and location of the cores.

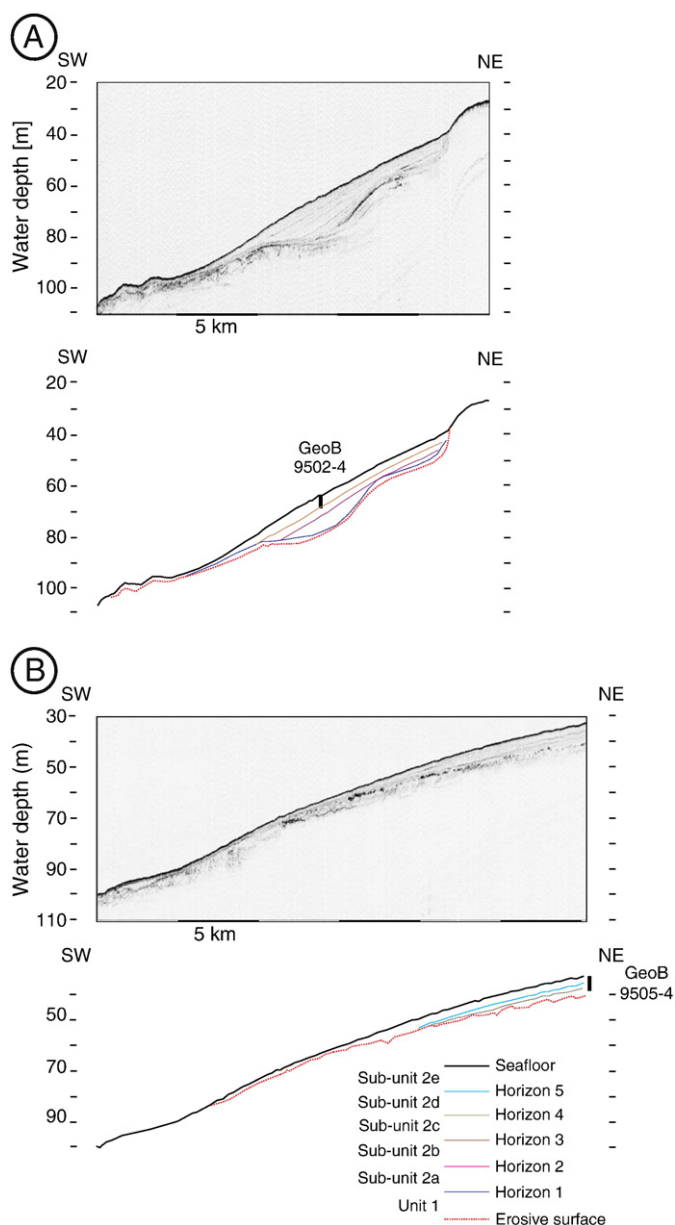


**Fig. 5.** Parasound profile of two transversal transects (Fig. 1A) from the northern (A) and the southern (B) regions of the MB. An interpretation of the deposit architecture is displayed below each profile as well as the length and location of the cores.

tremendous amount of terrigenous Fe input. We assume, therefore, that semi-quantitative data measured by the XRF core scanner for Fe are largely correct (Nizou et al., *in press*). Western Saharan dust displays particularly high percentages of  $\text{CaCO}_3$  compared to other dust sources over NW-Africa, values can reach up to ~18% (Moreno et al., 2006). Therefore we assume that the Ca offshore Senegal originates not exclusively but mainly from marine origin.

The grain-size distribution (GSD) of the terrigenous fraction was measured with a Beckman-Coulter Laser Particle Size Analyzer LS 200 (Fullerton, USA). One gram of sediment was retrieved in 2 to 10 cm-step intervals from Core 9503-5 and every 10 cm from the three other cores. Organic matter, carbonate and biogenic opal were removed by chemical treatment. Then, the remaining lithogenic fraction of the sediment was analyzed. The grain-size mode was automatically computed and the proportions in volume of clay (<2  $\mu\text{m}$ ), silt (2–63  $\mu\text{m}$ ) and sand (>63  $\mu\text{m}$ ) were calculated from the measured distributions.

Hierarchical cluster analysis was performed on the GSD from the individual cores with the aim of partitioning the samples into groups based on their similarity. The similarity between any given pair of samples was determined by the Aitchison distance separating them (Aitchison, 1982; Martín-Fernández et al., 1998). This measure of similarity is suitable for GSD which are fundamentally a 'closed' data type (i.e., each sample is subject to a constant-sum-constraint). The sample GSD were grouped progressively using the linkage technique of Ward (1963) and this process is displayed graphically in the form of dendrograms. Mean GSD were calculated for each cluster based upon the sequence with which the individual samples had been linked.

## 4. Results

### 4.1. Shallow-acoustic stratigraphy

The shallow-acoustic profiles show a wedge-shaped sedimentary body extending along the Senegalese coast in mid-shelf position (Figs. 1B, 4, 5). The upper border of this sedimentary body is the modern seafloor and its lower border is a strong, sharp and irregular discontinuity of high reflectivity (Figs. 4, 5). The overall sedimentary body is characterized by weak and diffuse internal reflections occasionally intercalated by parallel internal horizons of higher reflectivity. This sedimentary body pinches out in seaward direction at modern water depths of about 90 to 100 m (Figs. 4, 5). In NS directions, the body reaches its maximum thickness in the north (~17 m at core site 9502-4) and becomes progressively thinner towards the South (~7 m at core site 9505-4; Fig. 1B, 4).

Along the shallow-acoustic profiles, specific internal horizons (H) were mapped (Figs. 4, 5, 6) allowing the identification of two main MB units based on their acoustic facies and geometry.

The first and lower unit appears between the MB basal discontinuity and the reflector H1 (Figs. 4, 5, 6A). This unit, which only occurs in the northern part, consists of a chaotic acoustic facies which has a higher reflectivity than the unit above (Unit 2). Unit 1 drapes on the underneath irregular MB basal discontinuity and is in angular discordance with the overlying unit (Fig. 5A).

Unit 2 displays a weak to transparent internal reflection intercalated by medium-high-amplitude parallel horizons (Figs. 4, 5). Sub-units 2a, 2b, 2c, 2d and 2e were defined between H1–H2, H2–H3, H3–H4, H4–H5 and H5–the seafloor, respectively. Horizon H2 only appears in the northern part of the MB and on-laps the edge of a topographic low between core sites 9503-5 and 9504-3 (Figs. 4, 6B). Horizon H3, which occurs above this depression, can be traced until it on-laps the MB basal discontinuity between core sites 9504-3 and 9505-4 (Figs. 4, 6C). Horizons H4 and H5 only appear in the middle and southern regions of the MB, i.e. in front of the present river mouth location (Figs. 4, 6DE). Sub-units 2d and 2e pinch out on the seafloor between core sites 9503-5 and 9504-3 (Fig. 4).

In the cross-section profiles, an aggradational internal stacking pattern is characterized by parallel-oriented internal horizons (Fig. 4). This pattern transforms seaward into a progradational pattern with gently-sloping downlap terminations (Fig. 5B). However in the north around core site 9502-4, the horizons appear to have a higher dipping angle than in the other regions of the MB. A strong prograding depositional pattern is, thus, displayed (Figs. 4, 5A).

In the northern regions of the MB, between core sites 9502-4 and 9503-5 (Fig. 4), modifications in acoustic properties of the sub-seafloor data are observed. A distinct reflector situated between 6 and 8 m below seafloor is completely masking the reflectors beneath. This disappearance of reflections is considered as an acoustic blanking phenomenon. Above this reflector, enhanced reflections with coherent acoustic reflections having a higher amplitude in part of their extent are observed.

#### 4.2. $^{14}\text{C}$ dating, elemental stratigraphy based on Fe/Ca ratio and sedimentation rates

A total of 25 radiocarbon dates ranging from 4075 cal a BP [intercept age; 3999–4150 cal a BP;  $1\sigma$  probability range] to present were measured on the sediment gravity cores (Table 3; Fig. 7). Cores 9503-5 and 9504-3 display an age framework based on 10 and 7 AMS- $^{14}\text{C}$  ages respectively and provide, therefore, well-suited high-resolution sedimentary archives over the late Holocene. The age control of cores 9502-4 and 9505-4 is based on 3 and 4 AMS  $^{14}\text{C}$  ages, respectively. Although less accurate than the age control from cores 9503-5 and 9504-3, the sedimentary records from cores 9502-4 and 9505-4 provide valuable additional information in the following. From north to south the core tops are dated at 525 [513–532], 1225 [1179–1266] and 700 [678–725] cal a BP, while the southernmost core, just South of the modern position of the river mouth, shows modern sedimentation (Fig. 7). However, a discrepancy is observed between two core tops (9503-5 and 9504-3) and their two associated surface-preserving multi-cores (9503-3 and 9504-4) which suggest a modern sediment surface. This discrepancy can be due to the different coring techniques with the loss of the first centimeters of soft sediment during the gravity coring. As seen in the following, the very low sedimentation rates of the multi-cores compared to those of the gravity cores strengthen the decision of considering the first centimeters of surficial sediment as not being part of the MB sedimentation.

The core stratigraphy is established based on the variations in the XRF core scanner-derived Fe/Ca ratio as a function of age (Fig. 7). The Fe/Ca ratio fluctuations do not represent variations in absolute concentration but relative changes to each other. Core 9502-4 displays two intervals of high Fe/Ca values from 3400 to 2800 and from 2500 to 1900 cal a BP (Fig. 7A). Then from 1900 cal a BP onward values remain low and stable until the end of the sedimentary record at 525 cal a BP. Core 9503-5 shows a rather low and stable Fe/Ca ratio from 4100 to 2600 cal a BP, and a rather high and variable Fe/Ca ratio from 2600 to 1900 cal a BP (Fig. 7B). Then from 1900 cal a BP until the end of the record at 1225 cal a BP, values remain low. The Fe/Ca ratio of Core 9504-3 displays two periods of low values from 3010 to 2750 and from 1900 to 1000 cal a BP, and two main periods of high values from 2750 to 1900 and from 1000 to 700 cal a BP (Fig. 7C). Although core 9505-4 suffers from a lack of reliable dating at the beginning of the record, the values of Fe/Ca are low from 3800 to 3400 cal a BP and high from 3400 to 2600 cal a BP (Fig. 7D). Then values are low until the occurrence of a peak at 750 cal a BP. Finally, values are decreasing towards modern values.

The use of linear interpolation for the sedimentation rate automatically fixes sedimentation rate changes to the core depth where dates are located. However, it must be noted that dating points were chosen according to changes in the Fe/Ca ratios. The record of Core 9502-3 ends at 525 cal a BP and displays, with respect to the age framework, a rather low (20 cm/100 a) and stable sedimentation rate (SR; Fig. 8A). In contrast, Core 9503-5 which sedimentation record ends at 1225 cal a BP, displays a highly variable SR (from 10 to 160 cm/100 a; Fig. 8B). Four main changes in SR can be distinguished. From 4075 to 2685 cal a BP the SR was low and stable (10 cm/100 a), whilst from 2685 to 1855 cal a BP the SR was generally high associated with strong variations, then the SR became rather low from 1855 to 1350 cal a BP, until a final increase at 1350 cal a BP. The dating made on Multi-core 9503-3 indicates a very low SR from 1855 cal a BP until present (2 cm/100 a). The sedimentation record of Core 9504-3 ends at 700 cal a BP and displays three main SR changes (Fig. 8C). From 3010 to 1770 cal a BP a high SR (30 cm/100 a) prevails, then until 1120 cal a BP the SR decreases (10 cm/100 a), and rises again (40 cm/100 a) until the end of the record. Multi-core 9504-4 indicates a very

low SR from 575 cal a BP until present (8 cm/100 a). Core 9505-4 shows two major intervals of different SR levels: a low SR from 3480 to 1285 cal a BP and an elevated SR until present (Fig. 8D). The fact that multi-cores record very low sedimentation rates supports the hypothesis that only a few centimeters of sediment are missing.

#### 4.3. Grain-size distribution

##### 4.3.1. Downcore grain-size distribution

The modal grain size corresponding to the most abundant class in the GSD, together with the volume proportions of clay, silt and sand, are monitored downcore.

The Core 9502-4 grain-size mode shows two phases, a fine mode (5  $\mu\text{m}$ ) from 3250 to 1750 cal a BP and coarser mode (35  $\mu\text{m}$ ) from 1750 cal a BP onward (Fig. 8A). The core 9502-4 clay proportion displays, like the modal grain size, two phases, high values around 25 vol.% from 3250 to 2000 cal a BP and low values around 15 vol.% until the end of the record (Fig. 9A). From 4200 cal a BP onward, Core 9503-5 is characterized by a grain-size mode of 8  $\mu\text{m}$  which decreases to 5  $\mu\text{m}$  at 2700 cal a BP and remains stable until 2200 cal a BP. Then the mode fluctuates and increases until the end of the record (Fig. 8B). The proportion of clay follows the same pattern as the grain-size mode with prominently high values (25 vol.%) between 2700 and 2200 cal a BP (Fig. 9B). Core 9504-3 shows a fine grain-size mode (5  $\mu\text{m}$ ) prior to 2000 cal a BP which then increases drastically to 45  $\mu\text{m}$  (Fig. 8C). From 1100 cal a BP onward the grain-size mode decreases down to 32  $\mu\text{m}$ . The clay content is high in two parts of the 9504-3 record, from 3010 to 2000 cal a BP (22 vol.%), and for a brief interval around 1000 cal a BP (19 vol.%; Fig. 9C). With respect to the age framework, the exceptionally coarse-grained Core 9505-4 displays three main phases regarding the grain-size mode. From 4000 to 3250 cal a BP the mode displays a very coarse grain size (up to 250  $\mu\text{m}$ ), from 3250 to 2000 cal a BP the mode decreases to 80  $\mu\text{m}$ , and values remain around 50  $\mu\text{m}$  afterwards (Fig. 8D). The proportion of clay stays around 10 vol.% along the entire record. However, as expected from the exceptionally coarse grain sizes in this core, the proportion of sand is initially high with 75 vol.%, decreasing to 10 vol.% from 4000 to 2000 cal a BP, where the values remain until present day (Fig. 9D).

##### 4.3.2. Hierarchical cluster analysis of the raw grain-size distribution data

In order to allow a direct comparison between the four cores, the cutoff linkage distance at which the different clusters were defined in the dendrograms was set manually (Fig. 10). The cluster analysis results are considered to be robust given the realistic form and mode locations of the cluster mean GSD.

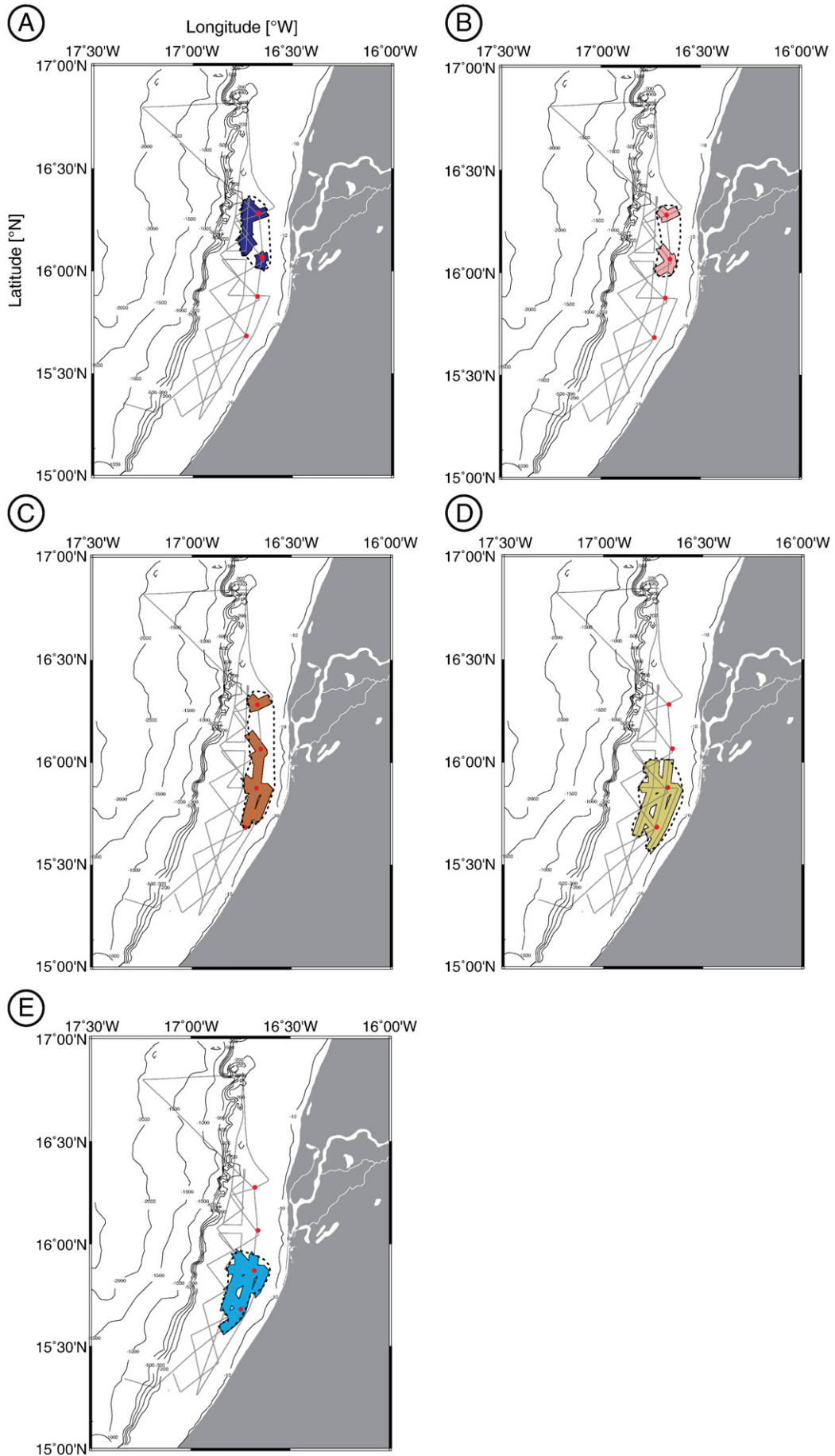
Each of the northernmost cores is represented using a three cluster model, with modes in the cluster mean GSD at  $\sim 6$ ,  $\sim 8$  and  $\sim 30$   $\mu\text{m}$  (Fig. 10A,B,C). The grain-size composition of the southernmost core, GeoB 9505-4, is, in contrast, represented using 5 clusters (Fig. 10D). In the two finest clusters, the peaks at  $\sim 6$  and  $\sim 8$   $\mu\text{m}$  are again observed, however the magnitude of the 30  $\mu\text{m}$ -peak is considerably reduced and the main average mode appears to shift towards 50  $\mu\text{m}$ . Cluster 4 is composed of samples from 510 to 400 cm and displays a polymodal GSD with a main contribution to the 80  $\mu\text{m}$ -mode. Cluster 5 is composed of only three samples from the core base and displays a polymodal GSD with a prominent contribution at 220  $\mu\text{m}$ .

#### 4.4. Interpretation

##### 4.4.1. Paleoclimatic signal

The suspended material transported by the Senegal River is essentially composed of fine-grained material (Gac and Kane, 1986; Fig. 11A). The mode at 6  $\mu\text{m}$  found in the MB cores is, thus, attributed

Fig. 6. Maps showing the location of the horizons: (A) H1; (B) H2; (C) H3; (D) H4; and (E) H5. Computed data are displayed by colour areas along the shallow-acoustic lines whilst interpolations are displayed in dashed lines. Core locations are shown from north to south: GeoB9502-4, 9503-5, 9504-3, 9505-4.



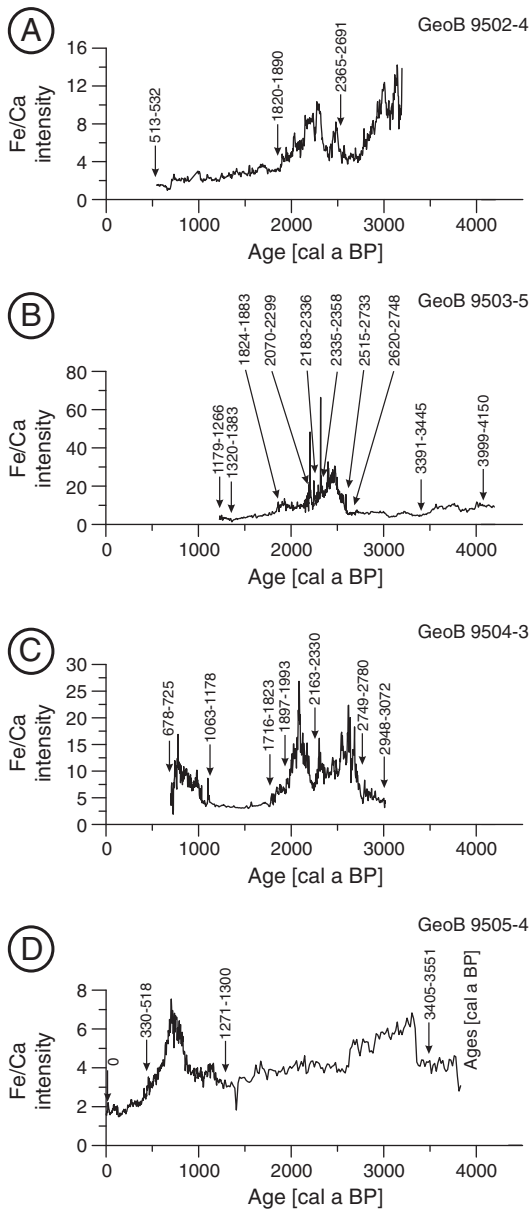


Fig. 7. Fe/Ca ratio from the XRF core scanner of the four cores plotted against age. Black arrows indicate the  $^{14}\text{C}$  dates.

to fluvial input. It must, however, be noted that when measured with Laser-based methods, the size of the clay particles is likely to be over-estimated (Konert and Vandenberghe, 1997). The GSD of the material collected by a shipboard dust sampler during Cruise M 65/1 in June 2005, during a period when Sahara Air Layer is dominant, displays an average mode of  $28\ \mu\text{m}$  (Fig. 10B). This allows the  $30\ \mu\text{m}$ -peak observed in the cores to be attributed to the aeolian component of the sediment. The dust material retrieved during Cruise M41/1 in February 1998, a time when the NE Trade Winds were dominant, shows, in contrast, an average modal grain size of  $9\ \mu\text{m}$  (Stuut et al., 2005; Fig. 11B). However, 5% of the river suspended particles also have a grain size in the range of 5 to  $10\ \mu\text{m}$  (Gac and Kane, 1986; Fig. 10A). We can, thus, assume that the  $8\ \mu\text{m}$ -mode is composed of a mixture of fluvial and aeolian material, which both have a similar grain-size signature.

Fluvial and aeolian sediments deposited off the Senegalese shelf show different elemental signatures. The fluvial material deposited in the MB is especially characterized by a high content in Fe derived from

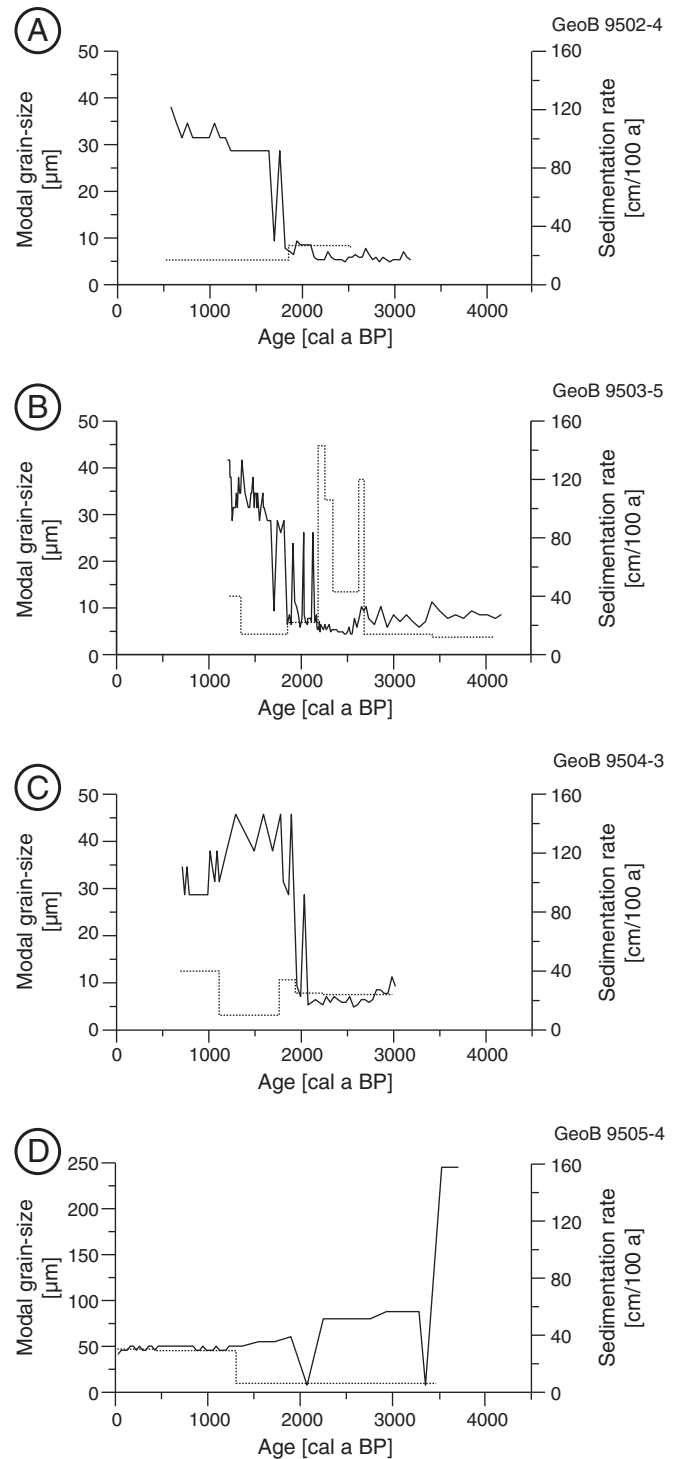
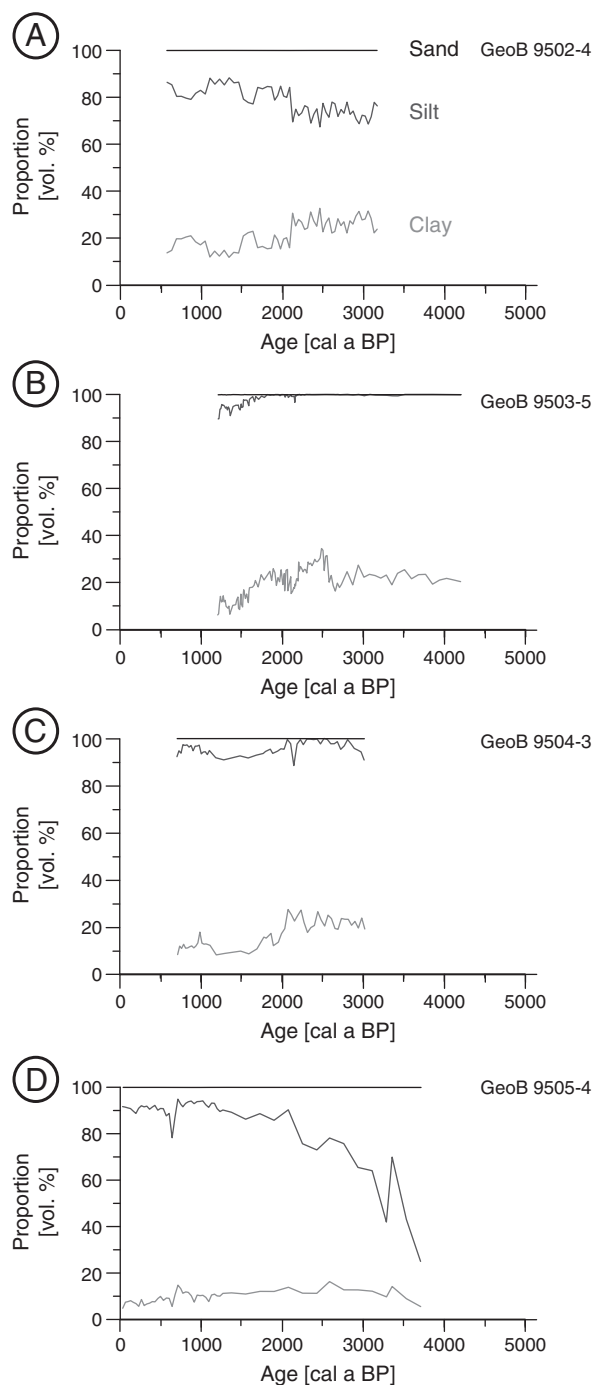


Fig. 8. Sedimentation rate (dashed line) and grain-size mode (black curve) of the four cores plotted against age.

the dominance of clay minerals (smectite, kaolinite, chlorite, illite and mixed-layer clays; Nizou et al., in press). Since the cores are situated in direct vicinity to the river mouth, the sedimentation rate should mainly depend on the river discharge. The terrigenous sediment discharged from the continent is thought to be controlled directly by climatic conditions in the hinterland. Thus, if we observe that the deposition of primary input material is not overprinted by secondary sedimentary processes or shifts in the river mouth location, then the



**Fig. 9.** Laser-based cumulative proportions of clay, silt and sand of the four cores plotted against age.

grain size, elemental distribution and sedimentation rate combined can be inferred as a paleoclimatic record. On the other hand, if the paleoclimatic history is known, changes over time in the local coastal to shallow-marine sedimentary regimes can be determined.

#### 4.4.2. Sedimentary processes suppressing the paleoclimatic signal

The southernmost core (GeoB 9505-4) shows average grain-size modes at  $\sim 80$  and  $\sim 220 \mu\text{m}$  (Fig. 10D). The modes correspond to the two coarsest hierarchical clusters (4 and 5) that are populated by samples exclusively from the base of the core. From 530 to 510 cm the

sedimentary facies is a mixture of grain sizes with various broken shell fragments from different mollusk species. This facies has the characteristics of a typical open-shelf relict deposit.

The  $50 \mu\text{m}$  mode, only displayed in GeoB 9505-4, cannot be related to wind input since the dust off Senegal displays finer grain sizes (Orange and Gac, 1990; Stuu et al., 2005). Due to the proximity of all core locations to each other, we assume that the input of dust, which takes place over wide areas and not in the form of a point source supply, would be displayed in all four cores with similar GSDs. We can exclude that this unusually coarse material displayed in a single core originates simply from an enhancement of the wind speed, because such a mechanism would have produced a coarsening also in the three other cores. This leads to the hypothesis that the coarse silts are not the result of primary input.

Core 9505-4 was retrieved in shallower water depth (36 mwd) than the three other cores and is located, according to Domain (1977), close to the region where the proportion of fine material is reduced compared to the northern part of the MB (Fig. 1A). The wave regime generally observed on the northern Senegalese shelf makes the reworking of sediment possible at a water depth of 36 m. A locally-restricted hydrologically-induced outbreaks/outwashes of material from local dunes and beach ridges can be responsible for the coarser grain sizes at this core site. We can, however, exclude large-scale erosion and incorporation of material originating from sand dunes into younger sediments during the Holocene transgression since such a mechanism would be also displayed in the other cores. All the cores originate from the shelf environment, and therefore are likely to be influenced by hydrological phenomena. The influence of changes in the coastal configuration on the cores will be discussed in the following.

#### 4.4.3. Specific aspect: linkage between free gas in the sediment and a buried depression feature

Enhanced reflection is characteristic for accumulation of gas in porous silt-rich sediments. Acoustic blanking reveals either migration of gas or absorption of acoustic energy in overlying gas-charged sediment (Judd and Hovland, 1992). In the northern part of the MB, the horizon which separates enhanced reflections (on top) from acoustic blanking (below) is inferred as top of free gas (Fig. 4).

The occurrence of free gas in organic-rich muds of shallow shelfal waters is a common phenomenon (see Fleischer et al., 2001 for a review). Potential sources for the formation of free gas in the shallow sub-bottom are the deposits rich in organic matter of the incised valley fills (Durán et al., 2007), buried estuaries (Marlow et al., 1996), and lakes and bogs (Gontz et al., 2002; Rogers et al., 2006). The blanking induced by the free gas in the sediment is likely to mask a possible buried depression structure which is filled with organic matter-rich sediments (Fig. 4). In the north, the prograding nature of the body displayed around core site 9502-4 (Figs. 4, 5A) together with the presence of a Senegal River meander observed in front of core site 9502-4 (Fig. 1A) hint to an ancient outlet of the Senegal River  $\sim 70$  km north of its present location. A paleo-channel is not directly displayed in the shallow-acoustic profiles, but such a topographic low can represent a lagoonal depression, a fluvial channel or a peat swale, as consequence of the adjacency to an old river mouth.

## 5. Discussion

### 5.1. Paleoclimatic history

A period of high sedimentation rate matching with high Fe/Ca ratios and small grain sizes is observed simultaneously in the three northernmost cores from 2750 to 1900 cal a BP indicating an increase in fluvial input (Figs. 7, 8, 9). This climatic change towards wetter conditions off Senegal is also documented through several other

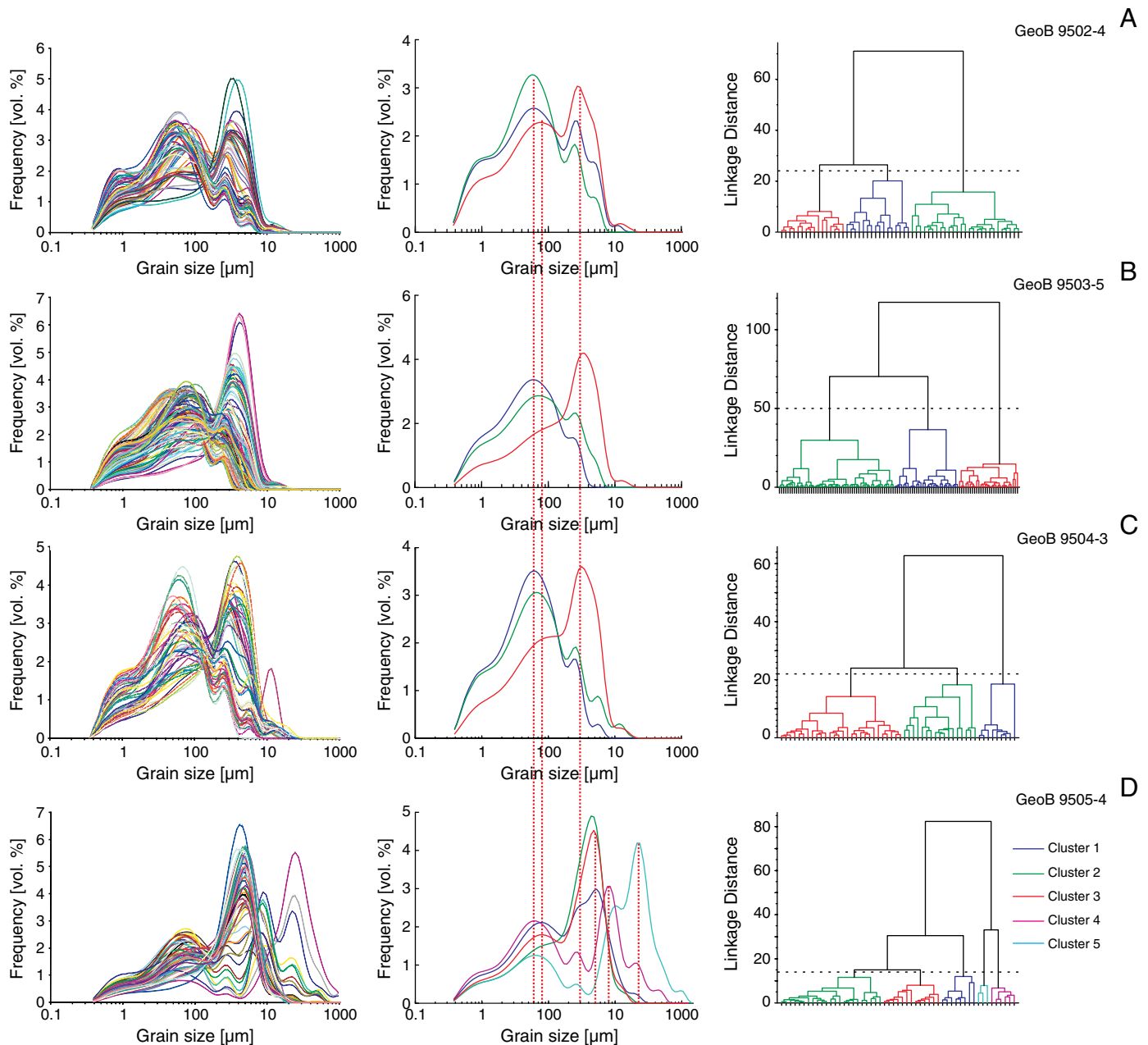


**Fig. 10.** Measured grain-size distribution data, mean grain-size distribution from the hierarchical cluster analysis and the associated dendrograms are shown for each core from left to right. The cutoff linkage distances in the dendrograms at which the different clusters were defined are shown by the dashed horizontal lines. For the hierarchical cluster analysis and the associated dendrograms different colors denote the individual clusters and their mean grain-size distribution. The left-to-right sequence of samples in the individual dendrograms is based on the sequence with which they were linked and is thus arbitrary.

records over NW-Africa. An absence of geomorphologic evidence for dune activation in Mali is recorded during this phase, which indicates humid conditions (Stokes et al., 2004). A humid episode is also recorded around the Sahara by fluvio-lacustrine deposition and aeolian sediment stabilization at about 3000 to 2000 cal a BP (Swezey, 2001). These findings are also in accordance with a rise in water level inferred from Lake Bosumtwi (Ghana; e.g., Talbot and Delibrias, 1980; Talbot et al., 1984; Gasse, 2000). Grain-size and elemental distribution data from a continental shelf depocenter off Mauritania also display a period of enhanced surface water runoff from 2600 to 1900 cal a BP (Hanebuth and Lantzsch, 2008). This humid interval matches also with the initial human occupation in the middle Senegal valley from 2750 to 2450 cal a BP (McIntosh, 2006).

Comparable evidences for elevated river discharge are shown in the two southernmost cores for the time interval from 1000 to 700 cal a BP. The timing of this second wet phase matches with a strongly reduced activation of dunes in Mali (Stokes et al., 2004), a rise in water level in Lake Bosumtwi (Gasse, 2000) and the initiation of a humid period in some lake records in Equatorial Africa (Alexandre et al., 1997; Vincens et al., 1998).

Core 9502-4 displays an interval of high Fe/Ca ratio dated by extrapolation around 3000 cal a BP regarding the age uncertainty (Fig. 7A). It could either be part of the wet interval observed from 2750 to 1900 cal a BP, or hint to an older wet phase. The high Fe/Ca values at the base of Core 9505-4 do not allow an interpretation without precise dating (Fig. 7D).

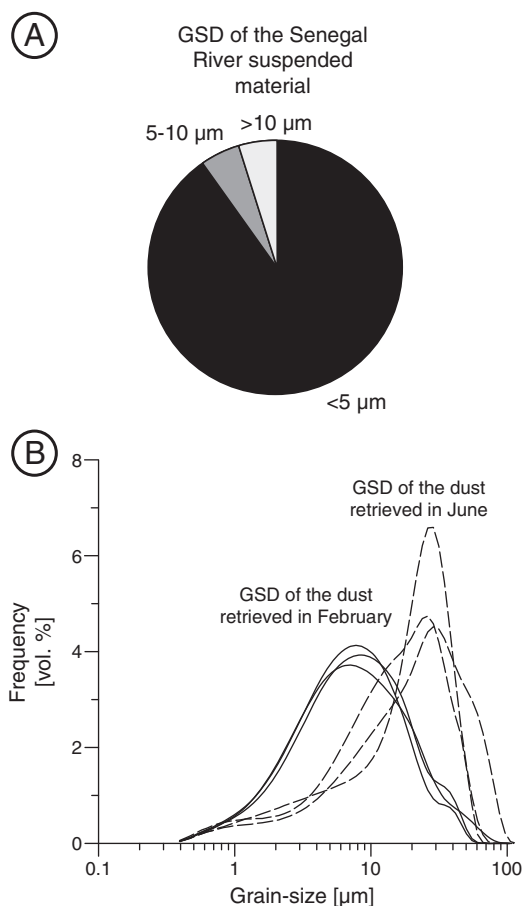


**Fig. 11.** (A) Grain-size distribution of the Senegal River suspended sediment (Gac and Kane, 1986). (B) Grain-size distribution of the dust retrieved off Senegal, in February during the cruise M41 (Stuut et al., 2005), and in June during the cruise M65.

## 5.2. Paleogeography

### 5.2.1. Pre-Holocene

The base of the MB is an irregular and rough discontinuity of high reflectivity which does not allow signal penetration beneath it (Figs. 4, 5). MB internal horizons onlap on this surface. Remarkably, this discontinuity displays the characteristics of an erosional surface and may be the result of exposure during the last sea-level lowstand.

On land, between the Last Glacial Maximum and the beginning of the African Humid Period, arid conditions prevailed (Mulitza et al., 2008; Barusseau et al., 2009). This period of aeolian dune construction is referred as “Ogolien” in the regional terminology (Swezey, 2003). The Senegal River did not reach the Atlantic Ocean because systems of red “Ogolien” dunes have blocked its course, which is consistent with the fact that no paleo-river channel intersecting the shelf was observed in the shallow-acoustic profiles.

### 5.2.2. Early Holocene

With the establishment of wet conditions in the Early Holocene, the Senegal River cut through the so-called “Ogolien” dune systems to reach the Atlantic Ocean (Michel and Durand, 1978), discharging heterogeneous sediments onto the Senegalese shelf (Fig. 12A).

In the northern regions of the MB, Unit 1 drapes the MB basal reflector (Figs. 4, 5, 6A). The chaotic acoustic facies of Unit 1 is interpreted as strongly heterogeneous sediments with variable grain sizes. Internal horizons of Unit 2 toplap and downlap onto Horizon 1 which account for an erosion of Unit 1. The chaotic acoustic facies of Unit 1 could be the result

of the intense shallow-water wave action which induced reworking and erosion of previously deposited terrestrial material.

Unit 2 displays different acoustic characteristics and, thus, suggests another depositional pattern than Unit 1. Sub-unit 2a only appears in the northern part of the MB (Fig. 6B). The absence of Sub-unit 2a in the southern regions of the MB accounts for a general pattern of deposition which started in the north. In contrast to the deposition of Unit 1 associated with strong reworking in shallow waters, the deposition of Unit 2 started when accommodation space was created below the wave-base level. Interestingly, the timing of the inception of mud deposition off Senegal seems in accordance with findings from Stanley and Warne (1994) describing, in several worldwide-distributed deltas, that favorable hydrological conditions for mud deposition are coeval with a slowdown in the rate of sea-level rise between 8500 and 6500 cal a BP. On land, humid conditions prevailed over NW-Africa during the so-called African Humid Period (e.g., deMenocal et al., 2000; Kröpelin et al., 2008) leading to an increase in fine fluvial discharge onto the shelf.

### 5.2.3. Mid and late Holocene

At the end of the post-glacial transgression, i.e. in mid-Holocene, the alluvial valley and the surrounding inter-dune subaerial depressions were flooded up to 250 km inland, leading to the formation of an elongated embayment (Michel and Durand, 1978; Barusseau et al., 2009; Fig. 12B). The estuarine conditions prevailing in the embayment must have led to fine-grained sedimentation taking place directly inside the bight associated with the development of mangroves (Barusseau et al., 2009).

From 4000 cal a BP onward, a weakened river discharge (Figs. 7, 8, 9; Bouimetarhan et al., 2009) favored the building of beach barriers near the present coastline by the wave-induced longshore currents (Fig. 12C; Michel and Durand, 1978). On the coast of Senegal, the elongated embayment was closed against the ocean and became progressively a protected lagoon. By this process, the deposits filling this lagoon must have formed the modern coastal lowland area. The wind-derived yellow dunes began to form during this arid episode (Figs. 7, 8, 9; Bouimetarhan et al., 2009; Barusseau et al., 2009).

At 2750 cal a BP, more humid conditions were established (Figs. 7, 8, 9) and led to an increase in the Senegal River runoff which built up a network of high levees. In-between these levees, depressions were filled with clay material originating from seasonal flooding (Michel and Durand, 1978). Due to the higher runoff, the fine alluvial material which was formerly deposited inside the lagoon has in parts been reworked, exported and finally deposited on the shelf.

### 5.2.4. Latest Holocene

From 1900 cal a BP onward, dryer conditions were established (Figs. 7, 8, 9). The Senegal River built up a meandering system. At this time, the former inter-levee depressions evolved into sabkha environments (Michel and Durand, 1978). Additionally, so-called present-day dunes progression and littoral drift have constructed beach barriers and sand spits (Langue de Barbarie) which have forced the Senegal River mouth towards the South (Michel and Durand, 1978).

Such on land observations are in accordance with shifts in depocenters observed offshore (Fig. 6D,E). The appearance of older sub-unit (2a) in the north and younger sub-units (2d and 2e) in the South account for a shift in the depocenters associated with an interruption of the sedimentation in the northern areas of the MB. Such a southward shift of the depocenter corresponds well with the core-top ages (Table 2). At present, the sedimentation is active in the southernmost area of the MB (9505-4) whilst sedimentation was already interrupted at sites 9503-5 and 9504-3 after 1225 and 700 cal a BP. A clear southward shift of the depocenter is, therefore, observed for the sub-recent period.

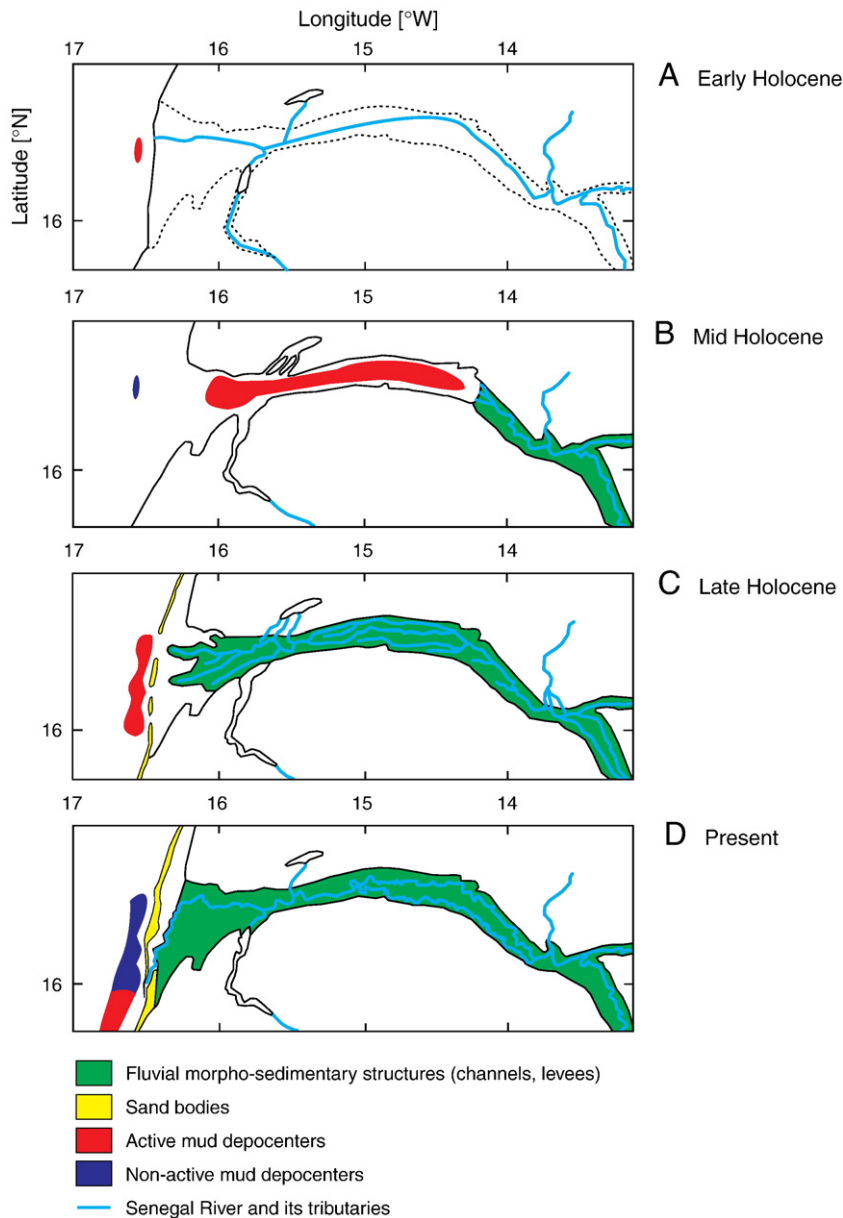


**Fig. 12.** Schematic paleogeography of the onshore and offshore Senegal River mouth system over the whole Holocene (modified after Michel, 1973). Late Holocene offshore reconstructions are derived from shallow-acoustic-based maps.

This recent cessation of the sedimentation in the northernmost areas of the shelf MB (Figs. 8, 12D) indicates either that the current regime flowing toward the north in summer does not contribute in a sufficient amount to the deposition on the MB, or that the winter current is able to remobilize sediments which were originally deposited during the summer season. Unfortunately, the resolution of our data does not allow us to reach a firm decision on this matter. Nevertheless, the component of the warm Equatorial Counter Current is known to be rather weak (~25 m/s; Domain and Bouille, 1976; Rebert, 1979). Since the sediment discharged from the river is not transported toward the north in a significant amount by the current conditions, the present-day extension of the MB, north of the actual river mouth location, can preferably be explained by an ancient river mouth which was located further to the north (Faure et al., 1980; Chamley and Diester-Haass, 1982). The recent shift towards the south is indeed confirmed by the very low sedimentation rates recorded by the two multi-cores (Table 3). The fact that the sedimentation at the northernmost areas has continued until 525 cal a BP, while it was

interrupted at 1225 and 700 cal a BP on southern areas implies that the Senegal River must have had several active outlets over a certain time interval. Such a scenario would fit well with the conditions of a progressively built-up sand barrier system which closed the lagoonal bight of the Senegal River.

## 6. Summary and conclusions

Elemental distributions, sedimentation rates and grain size investigations performed on cores retrieved from the Senegal MB allowed us to identify coastal and paleoclimatic changes. The fact that several cores were retrieved from the same sediment body gave us the ability, not only to emphasize a general paleoclimatic signal, but also to understand the coastal dynamics. Off the Senegalese shelf, terrigenous input is dominated by fine-grained Fe-rich fluvial material. Therefore, when the proportion of fine-grained material (clay vs silt and sand; low modal grain size values) rises together with Fe/Ca in several cores within the same period of time, we interpret

this phenomenon as an increase in river discharge. Two periods of higher river discharge, from 2750 to 1900 and from 1000 to 700 cal a BP, are displayed in the cores. These wet periods recorded off Senegal are coeval with climatic changes towards wetter conditions in other parts of NW-Africa. However, the periods of wetness are not recorded in the same way, and the intensity of the three proxies varies from one core to another. The differences in grain size from the southernmost core are not due to primary input but to stronger local hydrological conditions inducing remobilization of the sediment.

The base of the MB is a rough and irregular surface of erosion. This surface of erosion is believed to be the result of an exposure during the last sea-level lowstand. The upper border of the MB is the seafloor. Two main units were identified based on their acoustic facies and morphology. The chaotic Unit 1 draping on the irregular MB basal reflector is the product of sediment reworking. The strong hydrological energy conditions prevailing during the early phase of inundation caused the reworking and erosion of formerly deposited terrestrial coarse material in shallow-water depths. The overall Unit 2 displays a weak internal reflection with parallel internal horizons of medium-high reflexivity. The geometry and acoustic facies of Unit 2 indicate a different mode of sedimentation than Unit 1. The initiation of the mud deposition has started when the water cover was deeper than the wave base.

A slowdown in sea-level rise during the Early Holocene associated with the high river discharge led to mud deposition in the northern regions of the MB. During the mid-Holocene, a marine incursion has led to the formation of a large embayment extending up to 250 km inland. The presence of older sub-units in the north and younger sub-units in the south indicates a migration of the depocenters towards the South associated with an interruption of sedimentation in the north. This observation is confirmed by the core-top ages. During the late Holocene, the weak river discharge has allowed the longshore current to build a beach barrier system which forced the river mouth to shift towards the south.

## Acknowledgements

We want to thank the two reviewers who have improved the manuscript significantly. This work was funded through the Deutsche Forschungsgemeinschaft (DFG-Research Center)/Excellence Cluster "The Ocean in the Earth System".

## References

- Aitchison, J., 1982. The statistical analysis of compositional data (with discussion). *Journal of the Royal Statistical Society, Series B (Statistical Methodology)* 44 (2), 139–177.
- Alexandre, A., Meunier, J.-D., Lézine, A.-M., Vincens, A., Schwartz, D., 1997. Phytoliths: indicators of grassland dynamics during the late Holocene in intertropical Africa. *Palaeogeography, Palaeoclimatology, Palaeoecology* 136, 213–229.
- Ausseil-Badie, J., Barusseau, J.P., Descamps, C., Diop, E.H.S., Giresse, P., Pazdur, M., 1991. Holocene deltaic sequence in the Saloum estuary, Senegal. *Quaternary Research* 36, 178–194.
- Barusseau, J.P., Bâ, M., Descamps, C., Diop, S., Giresse, P., Saos, J.-L., 1995. Coastal evolution in Senegal and Mauritania at 10<sup>3</sup>, 10<sup>2</sup> and 10-year scales: natural and human records. *Quaternary International* 29 (30), 61–73.
- Barusseau, J.P., Bâ, M., Descamps, C., Diop, S., Diouf, B., Kane, A., Saos, J.-L., Soumaré, A., 1998. Morphological and sedimentological changes in the Senegal River estuary after the construction of the Diama dam. *Journal of African Earth Sciences* 26, 317–326.
- Barusseau, J.P., Vernet, R., Saliège, J.F., Descamps, C., 2007. Late Holocene sedimentary forcing and human settlements in the Jerf el Oustani-Ras el Sass region (Banc d'Arguin, Mauritania). *Geomorphologie-Relief Processus Environnement* 1, 7–18.
- Barusseau, J.P., Roger, J., Noel, B.J., Serrano, O., Duval, C., 2009. Notice explicative de la carte géologique du Sénégal à 1/200 000, feuilles de Saint-Louis-Dagana, Podor-Saldé, Matam-Semmé, Ministère des Mines, de l'Industrie et des PME, Direction des Mines et de la Géologie, Dakar. 55 p.
- Bouimetarhan, I., Dupont, L., Schefuß, E., Mollenhauer, G., Mulitza, S., Zonneveld, K., 2009. Palynological evidence for climatic and oceanic variability off NW Africa during the late Holocene. *Quaternary Research* 72, 188–197.
- Chamley, H., Diester-Haass, L., 1982. Effets du déplacement de l'embouchure du fleuve Sénégal, au Quaternaire supérieur, sur la sédimentation de la marge ouest-africaine. *Comptes Rendus de l'Académie des Sciences de Paris*, 295, 673–678.
- Clark, J.A., Farrell, W.E., Peltier, W.R., 1978. Global changes in postglacial sea level: a numerical calculation. *Quaternary Research* 9, 265–278.
- deMenocal, P., Ortiz, J., Guilderson, T., Adkins, J., Sarntheim, M., Baker, L., Yarusinsky, M., 2000. Abrupt onset and termination of the African Humid Period: rapid climate responses to gradual insolation forcing. *Quaternary Science Reviews* 19, 347–361.
- Domain, F., 1977. Carte sédimentologique du plateau continental sénégalais. Extension à une partie du plateau continental de la Mauritanie et de la Guinée Bissau. O.R.S.T.O.M., Paris.
- Domain, F., Bouille, 1976. Les fonds de pêche du plateau continental Ouest-africain entre 17° et 12°N. Institut sénégalais de recherche africaine 61.
- Durán, R., García-Gil, S., Díez, R., Vilas, F., 2007. Stratigraphic framework of gas accumulations in the Ría de Pontevedra (NW Spain). *Geo-Marine Letters* 27, 77–88.
- Faure, H., Fontes, J.C., Hebrard, L., Monteillet, J., Pirazzoli, P.A., 1980. Geoidal change and shore-level tilt along Holocene estuaries: Sénégal River Area, West Africa. *Science* 210, 421–423.
- Fleischer, P., Orsi, T.H., Richardson, M.D., Anderson, A.L., 2001. Distribution of free gas in marine sediments: a global overview. *Geo-Marine Letters* 21, 103–122.
- Gac, J.Y., Kane, A., 1986. Le fleuve Sénégal: I. Bilan hydrologique et flux continentaux de matières particulaires à l'embouchure. *Sciences Géologiques Bulletin* 39, 99–130.
- Gasse, F., 2000. Hydrological changes in the African tropics since the Last Glacial Maximum. *Quaternary Science Reviews* 19, 189–211.
- Gontz, A.M., Belknap, D.F., Kelley, J.T., 2002. Seafloor features and characteristics of the Black Kedges Area, Penobscot Bay, Maine USA. *Journal of Coastal Research* 36, 333–339.
- Grant, J.A., Schreiber, R., 1990. Modern swath sounding and sub-bottom profiling technology for research applications: the atlas hydrosweep and parasound systems. *Marine Geophysical Researches* 12, 9–19.
- Grossman, E.E., Eitrem, S.L., Fieldand, M.E., Wong, F.L., 2006. Shallow stratigraphy and sedimentation history during high-frequency sea-level changes on the central California shelf. *Continental Shelf Research* 26, 1217–1239.
- Hanebuth, T.J.J., Lantzsich, H., 2008. A Late Quaternary sedimentary shelf system under hyperarid conditions: unravelling climatic, oceanographic and sea-level controls (Golfe d'Arguin, Mauritania, NW Africa). *Marine Geology* 256, 77–89.
- Haworth, R.J., Baker, R.G.V., Flood, P.G., 2002. Predicted and observed Holocene sea-levels on the Australian coast: what do they indicate about hydro-isostatic models in far-field sites? *Journal of Quaternary Science* 17, 581–591.
- Judd, A.G., Hovland, M., 1992. The evidence of shallow gas in marine sediments. *Continental Shelf Research* 12 (10), 1081–1096.
- Konert, M., Vandenbergh, J., 1997. Comparison of laser grain size analysis with pipette and sieve analysis: a solution for the underestimation of the clay fraction. *Sedimentology* 44, 523–535.
- Kröpelin, S., Verschuren, D., Lézine, A.-M., Eggermont, H., Cocquyt, C., Francus, P., Cazet, J.-P., Fagot, M., Rumes, B., Russell, J.M., Darius, F., Conley, D.J., Schuster, M., von Suchodoletz, H., Engstrom, D.R., 2008. Climate-driven ecosystem succession in the Sahara: the past 6000 years. *Science* 320, 765–768. doi:10.1126/science.1154913.
- Lambeck, K., 2002. Sea level change from mid Holocene to recent time: an Australian example with global implications. In: Mitrovica, J.X., Vermeersen, B.L.A. (Eds.), *Ice Sheets, Sea Level and the Dynamic Earth: Geodynamics series*, 29. 33–50 p.
- Leroux, M., 2001. The meteorology and climate of tropical Africa. Springer, p. 493.
- Marlow, M.S., Hart, P.E., Carlson, P.R., Childs, J.R., Mann, D.M., Anima, R.J., Kayen, R.E., 1996. Misinterpretation of lateral acoustic variations on high-resolution seismic reflection profiles as fault offsets of Holocene bay mud beneath the southern part of San Francisco, Bay California. *Marine and Petroleum Geology* 13, 341–348.
- Martín-Fernández, J.A., Barceló-Vidal, C., Pawlowsky-Glahn, V., 1998. Measures of difference for compositional data and hierarchical clustering methods. In: Buccianti, A., Nardi, G., Potenza, R. (Eds.), *Proceedings of IAMG'98, The Fourth Annual Conference of the International Association for Mathematical Geology: De Frede*, pp. 526–531. Naples.
- Masse, J.P., 1968. Contribution à l'étude des sédiments actuels du plateau continental de la région de Dakar. Essais d'analyse de la sédimentation biogène. Rapport du Laboratoire de Géologie de la Faculté des Sciences de l'Université de Dakar 23.
- McIntosh, S.K., 2006. The Holocene Prehistory of West Africa: 10,000–1000 BP. In: Akyeampong, E. (Ed.), *Themes in West Africa's History*, pp. 11–32.
- McTainsh, G.H., Walker, P.H., 1982. Nature and distribution of Harmattan dust. *Geomorphology* 26, 417–435.
- Michel, P., 1973. Géologie des régions traversées par les fleuves Sénégal et Gambie, géomorphologique map. Mémoire ORSTOM, Paris, France.
- Michel, P., Durand, J.H., 1978. La vallée alluviale du Sénégal (Afrique de l'Ouest). Relations géomorphologie – sols – aptitudes culturelles et leur cartographie au 1/50,000. CATENA 5, 213–225.
- Monteillet, J., 1988. Environnements sédimentaires et paléocologie du Sénégal au Quaternaire. Ph.D. thesis, Univ. of Perpignan, France.
- Monteillet, J., Faure, H., Pirazzoli, P.A., Ravise, A., 1981. Invasion saline du Ferlo (Sénégal) à l'Holocène supérieur (1900 BP). *Palaeogeography of Africa* 13, 205–215.
- Moreno, T., Querol, X., Castillo, S., Alastuey, A., Cuevas, E., Herrmann, L., Mounkaila, M., Elvira, J., Gibbons, W., 2006. Geochemical variations in aeolian mineral particles from the Sahara-Sahel dust corridor. *Chemosphere* 65, 261–270.
- Mulitza, S., Bouimetarhan, I., Brüning, M., Freeseemann, A., Gussone, N., Filipsson, H., Heil, G., Hessler, S., Jaeschke, A., Johnstone, H., Klann, M., Klein, F., Küster, K., März, C., McGregor, H., Minning, M., Müller, H., Ochsenhirt, W.-T., Paul, A., Schewe, F., Schulz, M., Steinlöhnner, J., Stuut, J.-B., Tjallingii, R., Dobeneck, T.v., Wiesmaier, S., Zabel, M., Zonneveld, K., 2005. Report and Preliminary Results of Meteor-Cruise M65/1, Dakar-Dakar. 11.06.–1.07.2005. Univ. of Bremen, Germany, p. 149.

- Multiza, S., Prange, M., Stuut, J.-B.W., Zabel, M., Dobeneck, T.V., Itambi, A.C., Nizou, J., Schulz, M., Wefer, G., 2008. Sahel megadroughts triggered by glacial slowdowns of Atlantic meridional overturning. *Paleoceanography*. doi:10.1029/2008PA001637.
- Nizou, J., Hanebuth, T., Vogt, C., in press. Deciphering signals of late Holocene fluvial and aeolian supply from a shelf sediment depocenter off Senegal (NW Africa), *Journal of Quaternary Science*.
- Orange, D., Gac, J.Y., 1990. Bilangéochimique des apports atmosphériques en domaines sahélien et soudano-guinéen d'Afrique de l'Ouest (bassins supérieurs du Sénégal et de la Gambie). *Géodynamique* 5, 51–65.
- Pinson-Mouillot, J., 1980. Les environnements sédimentaires actuels et quaternaires du plateau continental sénégalais (Nord de la presqu'île du Cap-Vert). Ph.D. thesis, Univ. of Bordeaux, France, pp. 106.
- Pirazzoli, P.A., Montaggioni, L.F., 1988. Holocene sea-level changes in French Polynesia. *Palaeogeography, Palaeoclimatology, Palaeoecology* 68, 153–175.
- Rebert, J.P., 1979. Aperçu sur l'hydrologie du plateau continental ouest-africain. De la Mauritanie à la Guinée. Rapport COPACE/PACE, série 78/10, p. 4.
- Rogers, J.N., Kelley, J.T., Belknap, D.F., Gontz, A., Barnhardt, W.A., 2006. Shallow-water pockmark formation in temperate estuaries: a consideration to origins in the western Gulf of Maine with special focus on Belfast Bay. *Marine Geology* 225, 45–62.
- Sarnthein, M., Tetzlaff, G., Koopmann, B., Wolter, K., Pflaumann, U., 1981. Glacial and interglacial wind regimes over the eastern subtropical Atlantic and North-West Africa. *Nature* 293, 193–196.
- Seibold, E., Fütterer, D., 1982. Sediment dynamics on the Northwest African continental margin. *The Ocean Floor, Bruce Heezen Commemorative Volume*, pp. 147–163.
- Stanley, D.J., Warne, A.G., 1994. Worldwide initiation of Holocene marine deltas by deceleration of sea-level rise. *Science* 265, 228–231.
- Stokes, S., Bailey, R.M., Fedoroff, N., O'Marah, K.E., 2004. Optical dating of aeolian dynamism on the West African Sahelian margin. *Geomorphology* 59, 281–291.
- Stuiver, M., Reimer, P.J., Bard, E., Beck, J.W., Burr, G.S., Hughen, K.A., Kromer, B., McCormac, G., van der Plicht, J., Spurk, M., 1998. INTCAL98 Radiocarbon Age Calibration, 24000–0 cal BP. *Radiocarbon* 40, 1041–1083.
- Stuut, J.-B.W., Zabel, M., Lavik, G., Schefuß, E., Rasmussen, V., Schneider, R.R., 2005. Provenance of present-day eolian dust collected off NW Africa. *Journal of Geophysical Research* 110, D04202. doi:10.1029/2004JD005161.
- Swezey, 2001. Eolian sediment responses to late Quaternary climate changes: temporal and spatial patterns in the Sahara. *Paleogeography Paleoclimatology Paleoecology* 167, 119–155.
- Swezey, 2003. Late Pleistocene and Holocene dune activity and wind regimes in the western Sahara Desert of Mauritania: comment and reply. *Geology* e18.
- Talbot, M.R., Delibrias, G., 1980. A new late Pleistocene–Holocene water-level curve for Lake Bosumtwi, Ghana. *Earth and Planetary Science Letters* 47, 336–344.
- Talbot, M.R., Livingstone, D.A., Palmer, D.G., Maley, J., Melack, J.M., Delibrias, G., Gulliksen, J., 1984. Preliminary results from sediments core from lake Bosumtwi, Ghana. *Palaeoecology of Africa* 16, 173–192.
- Vernet, R., 2007. Le golfe d'Arguin de la préhistoire à l'histoire – littoral et plaines intérieures. Collection PNBA no 3, Nouakchott.
- Vincens, A., Schwartz, D., Bertaux, J., Elenga, H., de Namur, C., 1998. Late Holocene climatic changes in western equatorial Africa inferred from pollen from Lake Sinnda, Southern Congo. *Quaternary Research* 50, 34–45.
- Ward, J., 1963. Hierarchical grouping to optimize an objective function. *Journal of the American Statistical Association* 58 (301), 236–244.
- Washington, R., Todd, M.C., Lizcano, G., Tegen, I., Flamant, C., Koren, I., Ginoux, P., Engelstaedter, S., Bristow, C.S., Zender, C.S., Goudie, A.S., Warren, A., Prospero, J.M., 2006. Atmospheric links between topography, wind, deflation, lakes and dust: the case of the Bodélé Depression, Chad. *Geophysical Research Letters* 33. doi:10.1029/2006GL025827.